Biosensors and Bioelectronics 144 (2019) 111643

Contents lists available at ScienceDirect

Biosensors and Bioelectronics

journal homepage: www.elsevier.com/locate/bios

Electrochemical immunosensor based on Ag^+-dependent CTAB-AuNPs for ultrasensitive detection of sulfamethazine

Mingyue Yang[a], Xiangyang Wu[a], Xialin Hu[b,*], Kun Wang[c], Can Zhang[d], Eric Gyimah[a], Salome Yakubu[a], Zhen Zhang[a,**]

[a] School of the Environment and Safety Engineering, Jiangsu University, Zhenjiang, 212013, China
[b] Key Laboratory of Yangtze River Water Environment, Ministry of Education, College of Environmental Science and Engineering, Tongji University, 1239 Siping Road, Shanghai, 200092, China
[c] The School of Chemistry and Chemical Engineering, Jiangsu University, Zhenjiang, 212013, China
[d] School of Food & Biological Engineering, Jiangsu University, Zhenjiang, 212013, PR China

ARTICLE INFO

Keywords:
Immunoassay
Sulfonamides
Signal amplification
Nanozyme
Electrochemical biosensor

ABSTRACT

An electrochemical biosensor was proposed utilizing an improved amplification strategy for the rapid detection of sulfamethazine (as a model target) in aquatic environments. In this competitive immunoassay, cetyltrimethylammonium bromide-capped gold nanoparticles (CTAB-AuNPs) were used as a signal amplifier and electrode matrix and coated with an antigen-antibody (Cag-Ab_1) specific binding system as a recognition unit for the target compound. In addition, silver nanoparticle labels were functionalized with dendritic fibrous nanosilica (DFNS@AgNPs) and decorated onto chitosan/single walled carbon nanohorn (CS/SWCNH)-modified glass carbon electrodes (GCEs), which improved the electron transfer rate and increased the surface area, enabling more coating antigens to be captured. Under acidic conditions, massive amounts of the Ag^+ bound to the surface of the AuNPs dissolved, and consequently, formed Ag^+@CTAB-AuNP complexes, which resulted in a distinctly improved peroxidase-like activity and enhanced current response. Furthermore, the destroyed Ab_1-Ab_2-DFNS conjugation greatly decreased the impedance, bringing about the amplification of the electrochemical signals. After optimization of the parameters, the proposed approach exhibited excellent performance, including good sensitivity (LOD, 0.0655 ng/mL) and satisfactory accuracy (recoveries, 79.02%–118.39%; CV, 3.18%–9.82%), which indicates the great potential of this strategy for the rapid detection of trace pollutants in the environments.

1. Introduction

In recent decades, the development of electrochemical enzyme-linked immunosorbent assay (ELISA)-based methods for trace pollutant analysis has attached significant interest owing to their advantages of high sensitivities, ease of measurement, and cost effectiveness (Felix and Angnes, 2018; Wen et al., 2017); most of these methods have been based on typical systems containing specific antibody-antigen recognition and electrochemically active signal tags triggered by the current or impedance response (Du et al., 2011; Li et al., 2008; Tang et al., 2008; Zhang et al., 2010). However, their applications have been limited due to inherent problems: (i) varied environmental conditions damage the assay performance because of the natural enzymes implemented as biocatalysts in the detection systems (Farka et al., 2018; Gao et al., 2007; Wei and Wang, 2013); (ii) the enzyme labels are not sufficiently close to the electrode, limiting the rate of the electron transfer reactions (Kokkinos et al., 2016); and (iii) excess protein molecules (antigens and antibodies) acting as insulating layers on the sensing platform attenuate the electron transfer between the labels and electrode surface (Arkan et al., 2015; Wan et al., 2011; Giroud et al., 2009).

To address these issues, nanozymes, which are defined as nanomaterials with enzyme-like properties (Attar et al., 2019; Huang et al., 2019; Wu et al., 2019), have been introduced into electrochemical biosensors in place of traditional natural enzymes. Au nanoparticles (AuNPs) can be used as a nanozyme because these metal nanomaterials show outstanding catalytic activity towards the reduction of hydrogen peroxide (H_2O_2)(Lin et al., 2014; Luo et al., 2006; Shah et al., 2015). Furthermore, their good biocompatibility and excellent conductivity also contribute to their excellent performance in electrochemical

* Corresponding author.
** Corresponding author.
E-mail addresses: xlhu@tongji.edu.cn (X. Hu), zhangzhen@ujs.edu.cn (Z. Zhang).

https://doi.org/10.1016/j.bios.2019.111643
Received 4 July 2019; Received in revised form 21 August 2019; Accepted 27 August 2019
Available online 31 August 2019
0956-5663/

biosensing (Deng et al., 2018; Jayakumar et al., 2018; Mani et al., 2009). Fang et al. fabricated a biosensor for the sensitive determination of α-fetoprotein based on the good peroxidase-like catalytic activity of AuNP@ZnO(Fang et al., 2017). Using Au@PtDNs combined with nanographene (NG)/Cu^{2+}, which would provide abundant active sites for catalyzing the reduction of H_2O_2, Lv et al. established an immunosensor with a limit of detection (LOD) of 0.167 pg/mL (Lv et al., 2018). Nevertheless, the improved sensitivity of the assays in the above literature benefited from the inherent catalytic performance of the utilized Au nanocrystal labels, and rarely involved analyte-induced tunable catalytic systems because metal ions can affect the peroxidase-like activity of AuNPs(Li et al., 2017; McVey et al., 2018). Recently, a study showed that after Ag^+, Bi^{3+}, or Pb^{2+} were deposited onto AuNPs, the particles displayed strong peroxidase-like activity (Lien et al., 2013). Meanwhile, it was reported that Ag^+ can be competitively combined with cetyltrimethylammonium bromide (CTAB) on the surface of CTAB-AuNPs, leading to the exposure of the AuNP surface and the enhanced catalytic performance of the compound (Zhang et al., 2018a). Due to their unique surface chemistry properties, AuNPs are a potential candidate for use as the amplifier of electrochemical biosensors.

Inspired by these considerations, an improved competitive biosensor was established using Ag^+-sensitive CTAB-AuNPs deposited onto the electrode surface and DFNS@AgNPs, which have a pH-responsive Ag^+ generating ability, were used to trigger the peroxidase-like activity of the CTAB-AuNPs for signal amplification (illustrated in Scheme 1). After a series of investigations on the method (parameter optimization, accuracy and reliability estimation), the established immunosensor was applied for the detection of sulfamethazine (SMZ) in environmental water samples.

2. Experimental section

2.1. Materials and apparatus

Morphologies of the prepared nanocomposite were characterized by transmission electron microscope (TEM, JEM-2100, JEOL, Japan), the scanning electron microscope (FE-SEM, JSM-7001F, JEOL, Japan) as well as energy dispersive X-ray spectrometer (EDX). X-ray photoelectron spectroscopy (XPS) measurements were surveyed on an Axis Ultra spectrometer (Kratos Analytical Ltd., Japan). Electrochemical measurements were performed by a conventional three-compartment electrochemical cell on CHI 660E electrochemistry workstation (Shanghai Chenhua instrument, China). Monoclonal antibody (MAb 4D11) and coating antigen (CS-OVA) were kindly provided by professor Zhanhui Wang in China Agriculture University, and detailed information is provided in Table S1. Other materials, chemical reagents and buffer solutions were listed in Supporting Information.

2.2. Preparation of CS/SWCNHs

The preparation of carboxylated SWCNHs was achieved according to a previously reported procedure (Zhang et al., 2010). Briefly, 40 mg of SWCNHs were dissolved in 60% HNO_3 and then sonicated for 1 h. Then, the mixture was heated to 140 °C for 12 h to generate SWCNHs with carboxyl groups, which were then centrifuged and washed three times. Finally, the precipitate was dissolved in 5 mL of ultrapure water containing 1% chitosan (CS). The CS/SWCNH solution was stored at room temperature until further use.

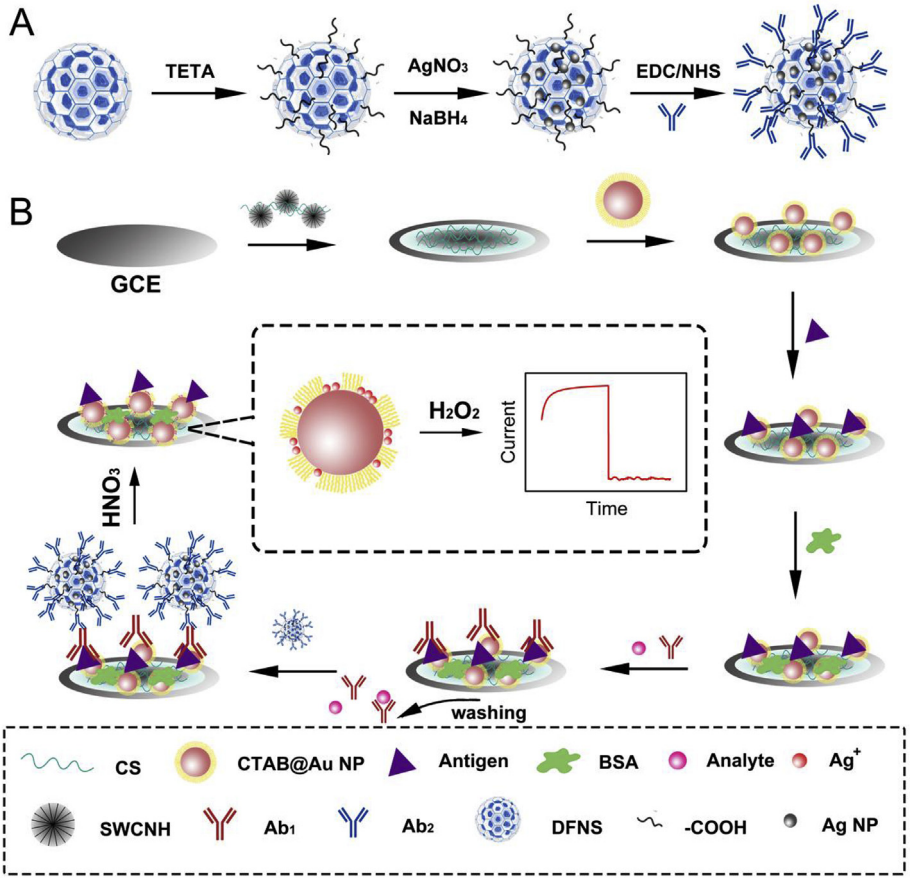

Scheme 1. Schematic illustration of the competitive immunosensor based on Ag^+@CTAB-AuNPs for detecting SMZ.

2.3. Synthesis of CTAB@AuNPs and construction of Ab_2-DFNS@AgNPs

To synthesize CTAB@AuNPs, a gold seed solution was first prepared as follows. A 0.2 M solution of $HAuCl_4$ (5 mL) was stirred together with 5 mL of a 0.5×10^{-3} M trisodium citrate solution. Then, 0.3 mL of an ice cold 0.1 M aqueous solution of $NaBH_4$ was added to the above solution under vigorous stirring. The solution was aged for 2 h at room temperature. Subsequently, the stock growth solution (150 mL, 0.25×10^{-3} M $HAuCl_4$, 80×10^{-3} M CTAB) was heated for 40 min, during which the color turned orange. Then, a three-step process was applied. First, to achieve solution I, 9 mL of the cooled growth solution was added to 50 μL of a 0.1 M ascorbic acid solution and 1.0 mL gold seed solution, after which the mixed solution turned reddish brown. Next, solution II was prepared by mixing 9 mL of the cooled growth solution, 50 μL of a 0.1 M ascorbic acid solution and 1 mL of solution I under vigorous stirring until a final red wine color was obtained. Finally, 90 mL of cooled growth solution was mixed with 500 μL of solution II at 70 °C. After cooling to room temperature and centrifugation (5000 rpm, 5 min), the CTAB@AuNPs were obtained.

The method for preparing Ab_2-DFNS@AgNPs conjugate was described in Supporting Information.

2.4. Fabrication of the sensor

Initially, the GCEs for the biosensor were successively polished with 0.3 and 0.05 μm alumina slurries, after which the electrodes were sequentially sonicated in ethanol and ultrapure water to remove residual alumina powder. Subsequently, a CS/c-SWCNH solution (6 μL) and CTAB-AuNP solution (6 μL) were sequentially added dropwise onto the pretreated GCEs and dried at room temperature. The resulting modified electrode (CTAB-AuNP/CS/c-SWCNH/GCE) was incubated with coating antigen (6 μL) overnight at 4 °C. After being washed 3 times with a washing buffer, the electrodes were blocked with a blocking buffer for 2 h at 37 °C. Then, 3 μL SMZ and 3 μL Ab_1 were deposited onto the above electrode and incubated for 30 min at 37 °C. As a result, a portion of the antibody was bound to the electrode via the antigen, and the residual conjugate compounds (antibody-SMZ) and SMZ were removed with a washing buffer. Then, 6 μL of the Ab_2-AgNP@c-DFNS bioconjugate was attached to the prepared electrode through specific binding, and excess antibody was removed by thorough rinsing. After acid treatment, the competitive immunosensor was measured in PBS (pH 7.4) with 25.0 mM H_2O_2.

2.5. Electrochemical measurements

For the detection of SMZ, current-time (I-t) measurements were carried out in 10 mL PBS (pH 7.4) solutions at room temperature with 25.0 mM H_2O_2 at an applied potential of 0.8 V. Cyclic voltammetry (CV) measurements were performed in PBS (pH 7.4) containing 100 mM H_2O_2 over a scanning potential range from −1.2 to −0.2 V at a scan rate of 25 mV/s. PBS (pH 7.4) with 5.0 mM $[Fe(CN)_6]^{3-/4-}$ and 0.1 M KCl was used as the electrolyte for electrochemical impedance spectroscopy (EIS).

3. Results and discussion

3.1. Characterization of the nanomaterials

The morphologies of the obtained materials were characterized by scanning electron microscopy (SEM) and transmission electron microscopy (TEM). CTAB-AuNPs were synthesized with a seed-mediated method in the presence of Au(III) and CTAB according to a reported procedure (Zhang et al., 2018a). As shown in Fig. 1A and E, the CTAB-AuNPs were smooth and spherical, with an average particle diameter size of 39 nm (size distribution histogram: 32–48 nm, displayed in Fig. 1F). Fig. 1B, C and 1D shows the elemental mapping results of Au, N and Br, indicating the homogeneous distribution of CTAB on the surface of the AuNPs. In addition, Fig. 1G demonstrates that the surface of the DFNS@AgNPs is rough; they have a diameter of approximately 80–100 nm, and numerous large radial meso-channels could also be observed on the surface. Furthermore, as shown in the TEM and SEM images (Figs. 1H and S1B), the DFNS@AgNP complexes were successfully synthesized, and DFNS was uniformly deposited onto the AgNPs.

Considering that the formation of the Ag^+@CTAB-AuNPs is the key factor for triggering the following reaction for signal amplification in the detection system, its formation was evaluated by X-ray photoelectron spectroscopy (XPS). Fig. 2A reveals that the binding peak of the Ag^+@CTAB-AuNP composition (84.03 V) was slightly shifted compared to that of the CTAB-AuNPs (84.23 V), suggesting that the binding energy peak of the Au $4f_{7/2}$ electrons was within the range of 83.5 (Au) to 85.0 eV (polynuclear Au(I)–ligand complex)(Lien et al., 2014; Wei et al., 2012). Fig. 2B displays that the Ag 3d spectrum of the AgNPs could be deconvoluted into two peaks (380.03 eV and 368.23 eV); in contrast, the Ag 3d spectrum of the Ag^+@CTAB-AuNP complex exhibited binding peaks at 379.78 eV and 367.83 eV, which demonstrated the ionic state of Ag^+ based on the difference value of ≈0.5 eV for Ag $3d_{5/2}$ (Feng et al., 2013). The above data indicated that Ag^+ was successfully bound to the surface of the AuNPs to form the Ag^+@CTAB-AuNP complexes.

3.2. Feasibility of the proposed immunosensor

To verify the feasibility of this signal amplification strategy, investigation of the electrochemical catalytic activities of the different electrode interfaces towards H_2O_2 was performed with CV. As displayed by curve a (Fig. 3A), a very low voltammetric current was observed for the bare GCE owing to the absence of an electrochemically active substance. After coating with CTAB-AuNPs and CTAB-AuNP/CS/SWCNHs, the current response progressively increased, implying that the CS/SWCNHs have excellent conductivity and play an important role in signal amplification. Furthermore, comparing the current curves of the electrode before and after treatment with Ag^+ (Fig. 3B), curve b exhibited a sharp peak that appeared −0.8 V when Ag^+ was added to the solution containing CTAB-AuNP/CS/SWCNHs, which was ascribed to the markedly improved H_2O_2 reduction after binding Ag^+ to the surface of the CTAB-AuNPs.

In addition, the peak current of the Ag^+@CTAB-AuNP/CS/SWCNHs is approximately 4 times that of the Ag^+@CTAB-AuNPs, demonstrating the role of the CS/SWCNHs in improving the assay sensitivity. At the same time, the influence on the current response of different biochemicals (e.g., antigens or antibodies deposited onto the electrode) was also tested (Fig. 3C). Under acidic conditions, an obvious reduction peak appeared at approximately −0.84 V, indicating that the conjugation between the antigen and Ab_1 was destroyed, resulting in the electric impedance of the electrode decreasing, which is conducive to improving the sensitivity of the method. During the process, the Ag^+@CTAB-AuNPs showed excellent catalytic capability. By comparison, the current significantly decreased when the antibody was retained on the electrode due to the formation of an insulating layer. All of these results affirmed that our design as an amplified biosensor was feasible for sensitively detecting a target compound.

3.3. Characterization of the modified electrodes

Fig. 3D shows the typical Nyquist plot for the stepwise modification of the GCE electrode in a 0.1 M KCl solution containing 5 mM $[Fe(CN)_6]^{3-/4-}$. The EIS curve of a bare GCE electrode displayed a small semicircle (curve a), which indicated the diffusion-controlled characteristics of the electrochemical process. After functioned with a layer of the CS/SWCNH composites (curve b), a decrease in the electron transfer resistance was observed because the SWCNHs facilitated the transport of the electrons of the redox moieties to the electrode. At the

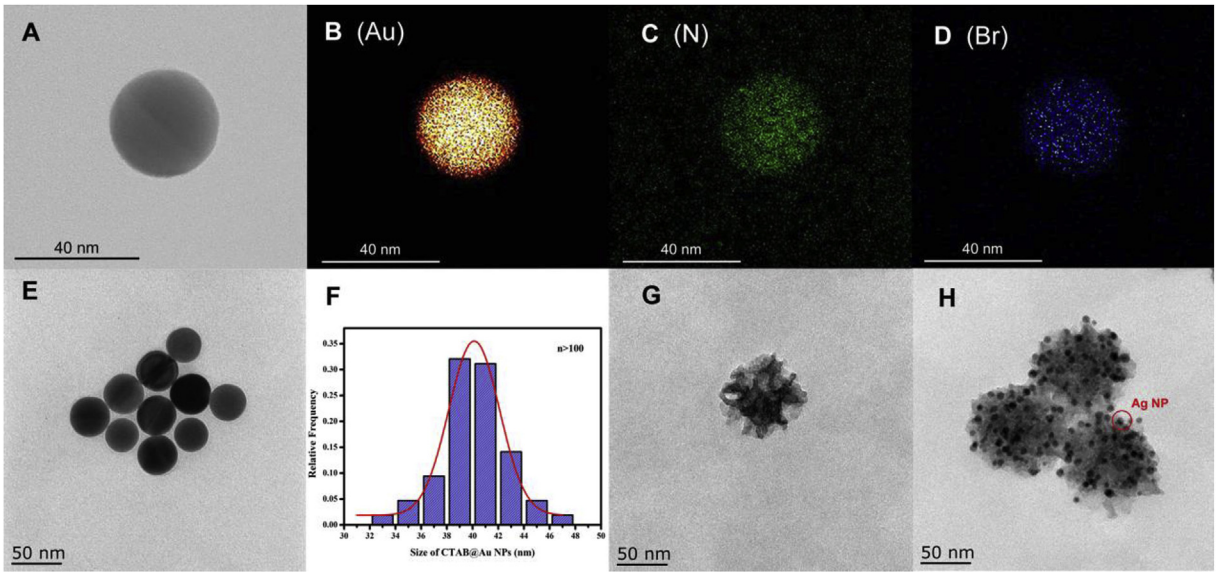

Fig. 1. HRTEM images of the CTAb-AuNP and EDX mapping images of Au (B), N (C) and Br (D). TEM images of the CTAB-AuNPs (D), DFNS (G) and DFNS@AgNPs (H). (F) The corresponding size distribution statistics of the CTAB-AuNPs from the TEM images (n ≥ 100).

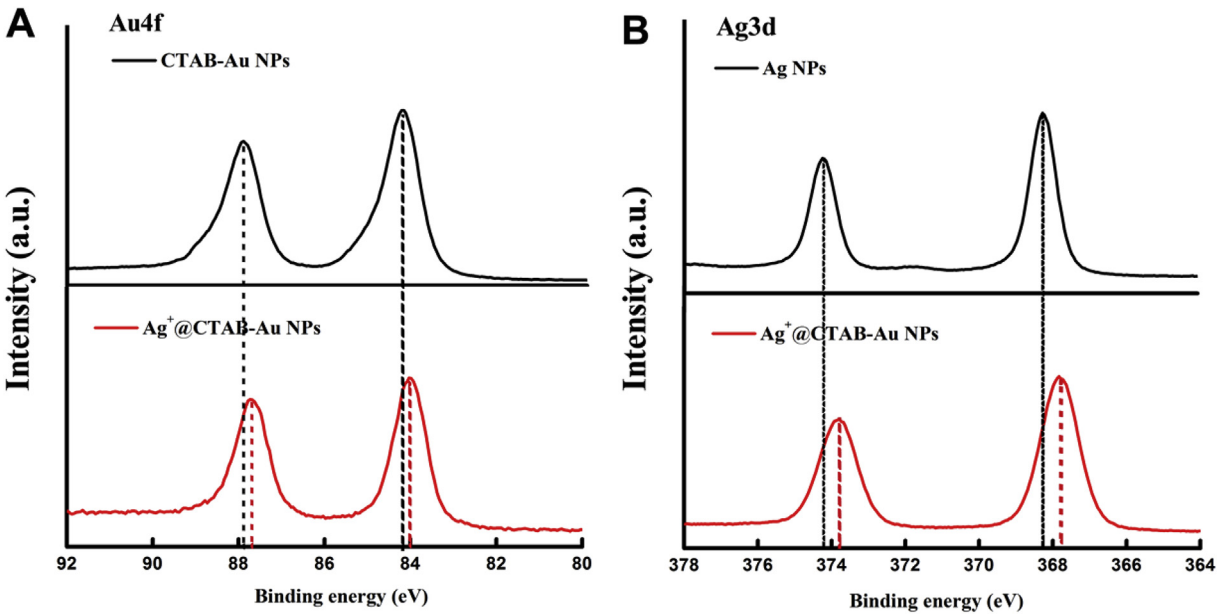

Fig. 2. (A) The core-level Au 4f XPS spectra of the CTAB-AuNPs (top) and Ag^+@CTAB-AuNP complex (bottom). (B) The core-level Ag 3d XPS spectra of the Ag NPs (top) and Ag^+@CTAB-AuNP complex (bottom).

same time, curve c revealed that the immobilization of a CTAB-AuNP layer further decreased the electron transfer resistance (from 103 Ω to 4.28 Ω) because of the reduced electrical conductivity of the metal material. The EIS curve increased after the electrodes were functioned with antigen, bovine serum albumin (BSA), and antibodies (curve d, e, and f, respectively), which was due to these biomolecules retarded the electron transfer rate between the redox probe and the electrochemical double layer (Dong et al., 2019; Liang et al., 2017; Zhang et al., 2018b). Besides, increased resistance (curve g) was observed because the modification layer (Ab_2-DFNS@AgNPs) hindered the diffusion of ferricyanide to the electrode surface. After the established electrode being treated with acid solution, the resistance decreased to 661 Ω because of loss of labels. The above measurements indicated that the immunosensor had been successfully fabricated.

3.4. Optimization of the parameters

Since some factors probably affect the constructed approach, like the concentrations of Cag/Ab_1/Ab_2-DFNS@AgNPs, recognition time, reaction time between Ag^+ and the CTAB-AuNPs, and pH value, these parameters were investigated in detail using I-t curves to obtain the best assay performance.

The reaction time between Ag^+ and the CTAB-AuNPs is a key factor, which likely affects the current response, and was first optimized within the range of 6–16 min. As shown in Fig. S3A, the current approached a stable value after a reaction time of 12 min, implying that 12 min was the optimal reaction time. Furthermore, Fig. S3B shows that the current gradually declined when Cag was diluted 8000-fold and then kept declination as Cag was diluted further. The maximum current value was observed when the dilution factor for Ab_1 was 6000 and that for the Ab_2-DNFS@AgNPs was 4 (Figs. S3C and D). Moreover, at pH value

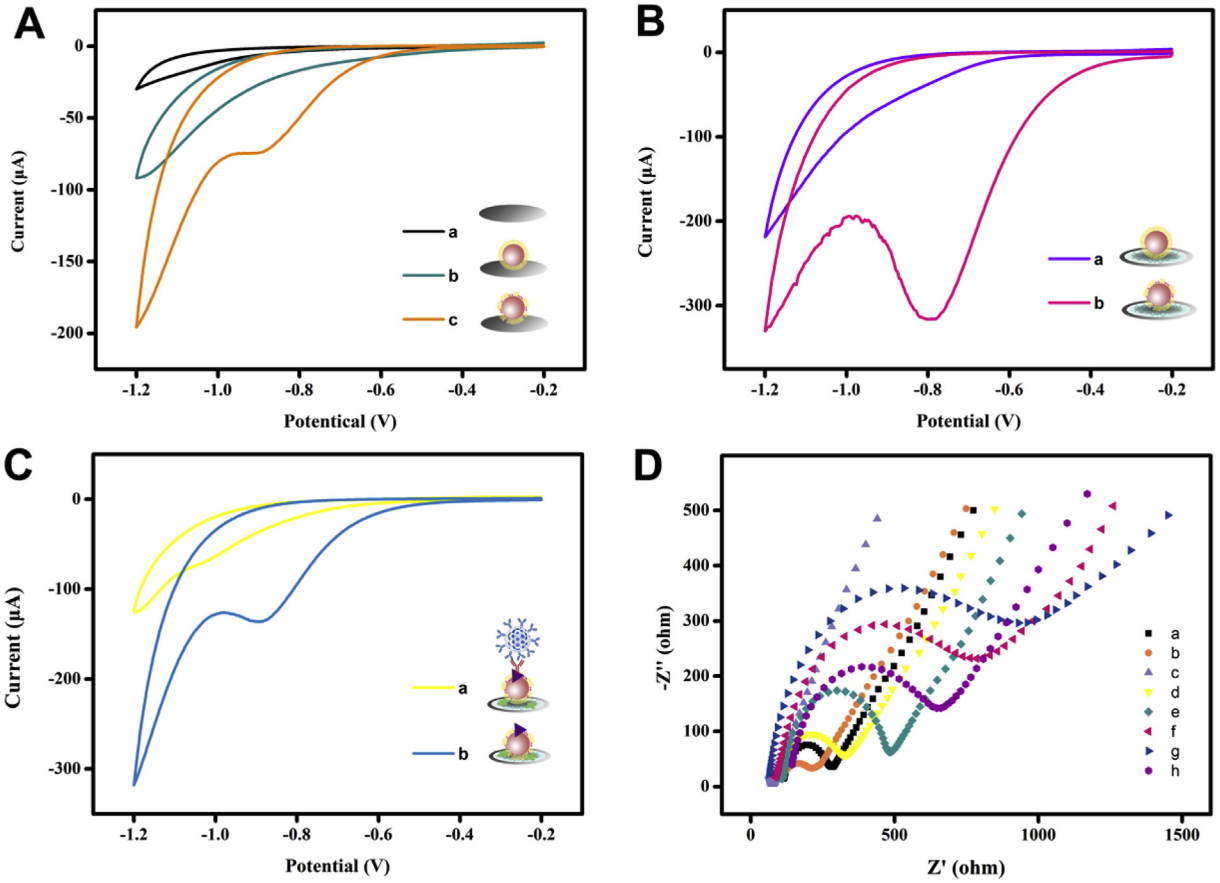

Fig. 3. CV voltammograms of (A) bare GCE (a), CTAB-AuNP/GCE (b), and Ag^+@CTAB-AuNP/GCE (c); (B) CTAB-AuNP/CS/SWCNH/GCE (a) and Ag^+@CTAB-AuNP/CS/SWCNH/GCE (b); and (C) Ab_2-DFNS/Ab_1/Cag/Ag^+@CTAB-AuNP/CS/SWCNH/GCE (a) and Cag/Ag^+@CTAB-AuNP/CS/SWCNH/GCE (b) in 10 mM PBS (pH 7.4) containing 100 mM H_2O_2. (D) EIS spectra of the modified bare GCE (a), CS/SWCNH/GCE (b), CTAB-AuNP/CS/SWCNH/GCE (c), Cag/CTAB-AuNP/CS/SWCNH/GCE (d), BSA/Cag/CTAB-AuNP/CS/SWCNH/GCE (e), Ab_1/BSA/Cag/CTAB-AuNP/CS/SWCNH/GCE (f), Ab_2-DFNS@AgNP/Ab_1/BSA/Cag/CTAB-AuNP/CS/SWCNH/GCE (g) and BSA/Cag/CTAB-AuNP/CS/SWCNH/GCE (f) in 0.1 M KCl aqueous solution containing 5.0 mM $[Fe(CN)_6]^{3-/4-}$.

ranged at 5–9, the best analytical performance was achieved at pH 7 (Fig. S3F). Thus, pH 7 was chosen as the optimal pH value for the immunoassay. In addition, the suitable recognition time between Ab_1 and the Ab_2-DNFS@AgNPs was found to be 40 min (Fig. S3E).

3.5. Sensitivity of the sensor

Under the above optimized conditions, the sensitivity of the proposed sensor was tested via I-t curves under serial concentrations of SMZ. As shown in Fig. 4A, the current response decreased with the increasing concentration of SMZ (from 0.05 ng/mL to 100 ng/mL). Notably, a good curve correlation was obtained between the incremental current ratio ($\Delta I/\Delta I_0$) and the logarithm of the concentration of SMZ (Log C_{SMZ}, ranging from 0.45 to 43.19 ng/mL) (Fig. 4B). The equation of the curve regression fit was $I/I_0 = 0.70246\ (1 + (\mathrm{Log}C_{SMZ}/1.06419)^{2.07746}) + 0.19968$, with a correlation coefficient of 0.997.

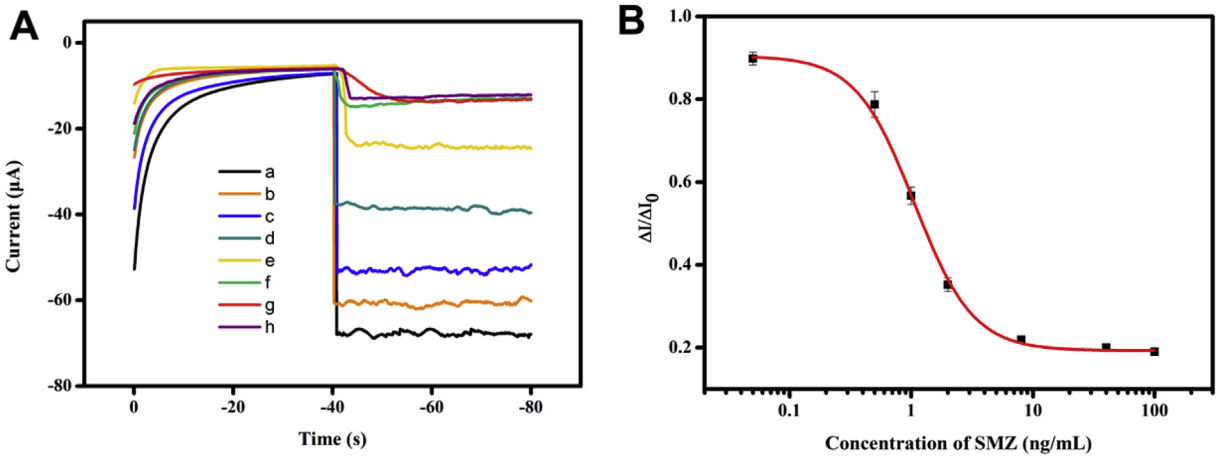

Fig. 4. (A) Current – time responses of the proposed immunosensor in 10 mM PBS (pH 7.4) containing 25 mM H_2O_2 to different concentrations of SMZ: 0.05, 0.5, 1, 2, 8, 40, and 100 ng/mL (a→h). (B) Calibration curve for SMZ detection.

Table 1
In-parallel analysis of real samples in Zhenjiang area by the established method and the conventional ELISA (n = 3).

Sapmle	ELISA (ng/mL)	This Method (ng/mL)	Relative error (%)
S1	ND[a]	0.092	–
S2	1.190	1.237	3.95
S3	0.487	0.502	3.08
S4	ND	0.152	–
S5	0.395	0.403	2.03

ND[a]: not be detected.

Accordingly, the LOD was calculated to be 0.0655 ng/mL (according to 90% inhibition)(Shelver et al., 2008), which was much lower than the limit when using an ELISA with the same antibody (Fig. S1), which indicated a distinct advantage of the proposed compared to the most of the reported sensors for SMZ detection (listed in Table S2).

3.6. Method validation and sample analysis

To assess the accuracy and precision of our method, spike-recovery analysis of various water samples (river waters, pure waters, lake waters, ponds waters and lake waters) was performed. As shown in Table S3, satisfactory recoveries (79.02%–118.39%) were obtained, and the intraassay coefficient of variation (CV) ranged from 3.18% to 9.82%. To further evaluate the reliability of this method, the established biosensor was applied to the analysis of real samples along with a conventional ELISA, and the results of the two methods were in good agreement (Table 1).

The investigation of the sensor accuracy and precision indicated that the proposed method is accurate and can be applied for the determination of trace chemicals in environmental water samples.

4. Conclutions

In summary, a novel electrochemical biosensor based on peroxidase-like Ag^+@CTAB-AuNPs was developed for the detection of SMZ (as a model target) in environmental water samples. The high sensitivity of this biosensor was ascribed to the amplification strategy as follows: (i) a remarkably increased current value due to the shortened distance between the nanozyme used and the electrode surface; (ii) the distinctly enhanced peroxidase-like activity of the CTAB-AuNPs towards the reduction of H_2O_2, which was triggered by the release of Ag^+; and (iii) the decreased electric impedance of the electrode caused by the destruction of the conjugation between the coating antigen and antibody-Ab_2-DFNS. Furthermore, the excellent repeatability and accuracy of the proposed method indicated its excellent potential for the rapid detection of SMZ, or other trace targets, by changing the antibody.

CRediT authorship contribution statement

Mingyue Yang: Conceptualization, Data curation, Formal analysis, Writing - original draft. **Xiangyang Wu:** Supervision. **Xialin Hu:** Funding acquisition. **Kun Wang:** Methodology. **Can Zhang:** Investigation. **Eric Gyimah:** Software. **Salome Yakubu:** Software. **Zhen Zhang:** Writing - review & editing.

Declaration of competing interest

The authors declare that they have no known competing financial interests or personal relationships that could have appeared to influence the work reported in this paper.

Acknowledgements

The present work was supported by the National Natural Science Foundation of China (Grants 21577051, 21876067, and 41601552).

Appendix A. Supplementary data

Supplementary data to this article can be found online at https://doi.org/10.1016/j.bios.2019.111643.

References

Arkan, E., Saber, R., Karimi, Z., Shamsipur, M., 2015. Anal. Chim. Acta 874, 66–74.
Attar, F., Shahpar, M.G., Rasti, B., Sharifi, M., Saboury, A.A., Rezayat, S.M., Falahati, M., 2019. J. Mol. Liq. 278, 130–144.
Deng, C., Zhang, M., Liu, C., Deng, H., Huang, Y., Yang, M., Xiang, J., Ren, B., 2018. Anal. Chem. 90 (19), 11446–11452.
Dong, S., Wang, S., Gyimah, E., Zhu, N., Wang, K., Wu, X., Zhang, Z., 2019. Anal. Chim. Acta 1048, 50–57.
Du, D., Wang, L., Shao, Y., Wang, J., Engelhard, M.H., Lin, Y., 2011. Anal. Chem. 83 (3), 746–752.
Fang, X., Liu, J., Wang, J., Zhao, H., Ren, H., Li, Z., 2017. Biosens. Bioelectron. 97, 218–225.
Farka, Z., Cunderlova, V., Horackova, V., Pastucha, M., Mikusova, Z., Hlavacek, A., Skladal, P., 2018. Anal. Chem. 90 (3), 2348–2354.
Felix, F.S., Angnes, L., 2018. Biosens. Bioelectron. 102, 470–478.
Feng, N., Wang, Q., Zheng, A., Zhang, Z., Fan, J., Liu, S.B., Amoureux, J.P., Deng, F., 2013. J. Am. Chem. Soc. 135 (4), 1607–1616.
Gao, L., Zhuang, J., Nie, L., Zhang, J., Zhang, Y., Gu, N., Wang, T., Feng, J., Yang, D., Perrett, S., Yan, X., 2007. Nat. Nanotechnol. 2 (9), 577–583.
Giroud, F., Gorgy, K., Gondran, C., Cosnier, S., Pinacho, D.G., Marco, M.-P., Sánchez-Baeza, F.J., 2009. Anal. Chem. 81, 8405–8409.
Huang, Y., Ren, J., Qu, X., 2019. Chem. Rev. 119 (6), 4357–4412.
Jayakumar, K., Camarada, M.B., Dharuman, V., Rajesh, R., Venkatesan, R., Ju, H., Maniraj, M., Rai, A., Barman, S.R., Wen, Y., 2018. ACS Appl. Mater. Interfaces 10 (25), 21541–21555.
Kokkinos, C., Economou, A., Prodromidis, M.I., 2016. TrAC Trends Anal. Chem. (Reference Ed.) 79, 88–105.
Li, X.-M., Yang, X.-Y., Zhang, S.-S., 2008. TrAC Trends Anal. Chem. (Reference Ed.) 27 (6), 543–553.
Li, X., Zhang, Y., Chang, Y., Xue, B., Kong, X., Chen, W., 2017. Biosens. Bioelectron. 92, 328–334.
Liang, Y.R., Zhang, Z.M., Liu, Z.J., Wang, K., Wu, X.Y., Zeng, K., Meng, H., Zhang, Z., 2017. Biosens. Bioelectron. 91, 199–202.
Lien, C.W., Chen, Y.C., Chang, H.T., Huang, C.C., 2013. Nanoscale 5 (17), 8227–8234.
Lien, C.W., Tseng, Y.T., Huang, C.C., Chang, H.T., 2014. Anal. Chem. 86 (4), 2065–2072.
Lin, Y., Ren, J., Qu, X., 2014. Adv. Mater. 26 (25), 4200–4217.
Luo, X., Morrin, A., Killard, A.J., Smyth, M.R., 2006. Electroanalysis 18 (4), 319–326.
Lv, H., Li, Y., Zhang, X., Gao, Z., Zhang, C., Zhang, S., Dong, Y., 2018. Biosens. Bioelectron. 112, 1–7.
Mani, V., Chikkaveeraiah, B.V., Patel, V., Gutkind, J.S., Rusling, J.F., 2009. ACS Nano 3, 585–594.
McVey, C., Logan, N., Thanh, N.T.K., Elliott, C., Cao, C., 2018. Nano Res 12 (3), 509–516.
Shah, J., Purohit, R., Singh, R., Karakoti, A.S., Singh, S., 2015. J. Colloid Interface Sci. 456, 100–107.
Shelver, W.L., Shappell, N.W., Franek, M., Rubio, F.R.J., 2008. J. Agric. Food Chem. 56, 6609–6615.
Tang, D., Ruo, Y., Chai, Y., 2008. Anal. Chem. 80, 1582–1588.
Wan, Y., Lin, Z., Zhang, D., Wang, Y., Hou, B., 2011. Biosens. Bioelectron. 26 (5), 1959–1964.
Wei, H., Wang, E., 2013. Chem. Soc. Rev. 42 (14), 6060–6093.
Wei, S.C., Hsu, P.H., Lee, Y.F., Lin, Y.W., Huang, C.C., 2012. ACS Appl. Mater. Interfaces 4 (5), 2652–2658.
Wen, W., Yan, X., Zhu, C., Du, D., Lin, Y., 2017. Anal. Chem. 89 (1), 138–156.
Wu, J., Wang, X., Wang, Q., Lou, Z., Li, S., Zhu, Y., Qin, L., Wei, H., 2019. Chem. Soc. Rev. 48 (4), 1004–1076.
Zhang, J., Lei, J., Xu, C., Ding, L., Ju, H., 2010. Anal. Chem. 82, 1117–1122.
Zhang, J., Zheng, W., Jiang, X., 2018a. Small. , e1801680.
Zhang, Z., Dong, S., Ge, D., Zhu, N., Wang, K., Zhu, G., Xu, W., Xu, H., 2018b. Biosens. Bioelectron. 105, 77–80.